Journal of Controlled Release 160 (2012) 692–698

Contents lists available at SciVerse ScienceDirect

Journal of Controlled Release

journal homepage: www.elsevier.com/locate/jconrel

# Hydrotropic magnetic micelles for combined magnetic resonance imaging and cancer therapy

Hong Yeol Yoon [a,b,1], Gurusamy Saravanakumar [a,1], Roun Heo [c], Seung Hong Choi [d], In Chan Song [d], Moon Hee Han [d], Kwangmeyung Kim [b,*], Jae Hyung Park [a,**], Kuiwon Choi [b], Ick Chan Kwon [b], Kinam Park [e]

[a] Department of Polymer Science and Engineering, Graduate School of Health Sciences and Technology, Sungkyunkwan University, Suwon 440–746, Republic of Korea
[b] Center for Theragnosis, Biomedical Research Institute, Korea Institute of Science and Technology, Seoul 136–791, Republic of Korea
[c] Department of Advanced Polymer and Fiber Materials, College of Engineering, Kyung Hee University, Gyeonggi-do 446–701, Republic of Korea
[d] Department of Radiology, Seoul National University College of Medicine, Seoul, Korea
[e] Departments of Pharmaceutics and Biomedical Engineering, Purdue University, West Lafayette, IN 47907, USA

ARTICLE INFO

*Article history:*
Received 16 January 2012
Accepted 5 April 2012
Available online 13 April 2012

*Keywords:*
Hydrotropic micelle
Magnetic resonance imaging
Paclitaxel
Drug delivery

ABSTRACT

Polymeric nanoparticles, capable of encapsulating imaging agents and therapeutic drugs, have significant advantages for simultaneous diagnosis and therapy. Nonetheless, improvements in the loading contents of the active agents are needed to achieve enhanced imaging and effective therapeutic outcomes. Aiming to make these improvements, a hydrotropic micelle (HM) was explored to encapsulate superparamagnetic iron oxide nanoparticles (SPIONs) as the magnetic resonance (MR) imaging agent and paclitaxel (PTX) as the hydrophobic anticancer drug. Owing to its hydrotropic inner core with hydrophobic nature, HM could effectively encapsulate both of PTX and SPION via the simple dialysis method. The hydrodynamic size of HM increased from 68 to 178 nm after physical encapsulation of SPION and PTX. Transmission electron microscopy analysis of HM bearing SPION and PTX (HM-SPION-PTX) revealed a spherical morphology with SPION clusters in the micelle cores. The micelles released PTX in a sustained manner. The bare HM and HM-SPION showed no toxicity to SCC7 cells, whereas HM-PTX and HM-SPION-PTX showed dose-dependent cytotoxicity that was lower than free PTX. HM-SPION-PTX exhibited 8.1-fold higher $T_2$ relaxivity than HM-SPION, implying potential of HM-SPION-PTX as the contrast agent for MR imaging. When systemically administered to tumor-bearing mice, HM-SPION-PTX was effectively accumulated at the tumor site, allowing its detection using MR imaging and effective therapy. Overall, these results suggested that HM-SPION-PTX is a promising candidate for combined diagnosis and treatment of cancer.



## 1. Introduction

Combining imaging and therapeutic capabilities into a single nanocarrier has garnered substantial attention because of the tremendous opportunity for simultaneous diagnosis and treatment of various diseases [1–3]. In particular, such combined nanoparticles allow real-time evaluation of therapeutic effects in vivo, which is critical for medical intervention through noninvasive methods. This approach has been studied using carrier systems such as liposomes, polymeric micelles, and polymersomes, and polymeric nanospheres [4–8]. Of various carriers, polymeric micelles based on amphiphilic block copolymers are an attractive choice for cancer imaging and therapy because of the availability of versatile polymerization techniques to control the molecular architecture, a well-defined core-shell structure capable of imbibing agents, prolonged circulation in the bloodstream, and high accumulation at the tumor site through an enhanced permeation and retention (EPR) effect [9].

Preparation of combined polymer micelles is similar to traditional drug loading methods. Imaging agents can be incorporated with drugs into micelles either by (i) direct conjugation of optical imaging labels (e.g., near infrared fluorescent dyes) or paramagnetic contrast agents (e.g., gadolinium) at the core or shell blocks; or (ii) co-encapsulation of hydrophobized contrast agents into micelle cores [4,10,11]. Although both of these loading methods have been studied for combined micellar systems, co-encapsulation of contrast agents and drugs by physical means into the hydrophobic cores of micelles is relatively easier than conjugation methods that require post-polymerization modification and complex chemistry [4,12].

In recent years, superparamagnetic iron oxide nanoparticles (SPIONs) have emerged as the magnetic resonance (MR) imaging agent because they are biocompatible and provide enhanced magnetic relaxivity, compared to the gadolinium complex [13]. The physical encapsulation of SPIONs into polymeric micelles results in formation of

* Corresponding author. Tel.: +82 2 958 5916; fax: +82 2 958 5909.
** Corresponding author. Tel.: +82 31 290 7288; fax: +82 31 290 7309.
*E-mail addresses:* kim@kist.re.kr (K. Kim), jhpark1@skku.edu (J.H. Park).
[1] These authors contributed equally to this paper.

0168-3659/$ – see front matter © 2012 Elsevier B.V. All rights reserved.
doi:10.1016/j.jconrel.2012.04.012

SPION clusters in the hydrophobic cores. The SPION-loaded micelles are generally water-dispersible and have the high colloidal stability. In addition, clustered SPIONs in micelles exhibit the high $T_2$ relaxivity and an enhanced contrast effect for precise MR imaging [14].

One of the critical problems, associated with conventional polymeric micelles, is their poor drug loading capacity and low stability [15]. This raises significant concerns for co-loading imaging agents with therapeutic drugs. Hence, efficient carrier systems with improved loading ability for dual-agent encapsulated micelles are critically needed. Recently, various block copolymer micelles have been investigated to trigger the release of active agents at the target site [16–18]. However, no substantial effort has been made to improve the loading capacity of active agents in a single-platform system, which is critical for enhanced imaging and effective therapy.

The drug loading capacity of polymeric micelles greatly depends on compatibility between the core-forming blocks and the drugs to be solubilized [15]. In this regards, amphiphilic block copolymer micelles have been synthesized with hydrotropes as the hydrophobic block [19,20]. Hydrotropes are small molecular amphiphiles that increase the aqueous solubility of poorly soluble agents. In screens of pharmaceutically safe hydrotropic agents, nicotinamide based hydrotrope (*N*,*N*-dimethylnicotinamide, DENA) was identified to specifically increase the aqueous solubility of paclitaxel (PTX) [21]. Hydrotropic block copolymer micelles, prepared using poly(ethylene glycol) monomethyl ether (PEG) as the hydrophilic block and DENA as the hydrotropic block, could encapsulate PTX up to 37.4% by weight [20]. Also, conjugation of oligomeric DENA to the backbone of polysaccharides such as chitosan and hyaluronic acid greatly increased the PTX solubility [22,23].

The main objective of this study was to explore a hydrotropic micelle (HM) as the single-platformed nanocarrier for simultaneous imaging and therapy. SPION and PTX co-loaded hydrotropic micelle (HM-SPION-PTX) was prepared using the simple dialysis method. The physicochemical characteristics of the micelles were investigated using dynamic light scattering (DLS) and transmission electron microscopy (TEM). The MR imaging contrast enhancement effect and tumor targetability of HM-SPION-PTX were also investigated using the tumor-bearing mice.

## 2. Materials and methods

### 2.1. Materials

PEG ($M_n = 5000$ Da), 2-hydroxynicotinic acid, diethylamine, vinylbenzyl chloride, and oleic acid were purchased from Sigma-Aldrich (St. Louis, MO, USA). PTX was kindly obtained from Samyang Genex Co. (Daejeon, Korea). All other reagents were of analytical grade and used as received. Amphiphilic hydrotropic block copolymer, PEG-*block*-poly(2-[4-vinylbenzyloxy]-*N*,*N*-diethylnicotinamide (PEG-*b*-P(VBODENA)), was synthesized according to a previously reported method via atom transfer radical polymerization (ATRP) [20]. The number-average molecular weight ($M_n$) of PEG-*b*-P(VBODENA), prepared in this study, was determined as 11,515 g/mol from $^1$H-NMR and 11,964 g/mol from gel permeation chromatography. Water used in all experiments was prepared by AquaMax-Ultra water purification system (Anyang, Korea).

### 2.2. Preparation of HM-SPION-PTX

Oleic acid-coated SPION was synthesized by a thermal decomposition method according to Park et al. [24]. In brief, iron–oleate complex, synthesized by using ferrichloride hexahydrate and sodium oleate, was reacted with oleic acid at 320 °C for 40 min, followed by precipitation in ethanol and centrifugation. For loading experiments, stock solution was prepared by dispersing 20 mg of SPION in tetrahydrofuran at a concentration of 1 mg/ml.

HM-SPION-PTX was prepared via simple dialysis method. PEG-*b*-P(VBODENA) block copolymer (40 mg) and PTX (12 mg) were dissolved in dimethylformamide (4 ml) and 2 ml of SPION solution was added drop wise, followed by vigorous stirring. After 30 min, 10 ml of distilled water was added slowly under sonication. The resulting solution was subjected to dialysis (MWCO = 3500 Da) against distilled water for 24 h. Afterwards, the solution was passed through an 0.8 μm cellulose acetate filter to remove large aggregates and unloaded materials. Consequently, HM-SPION5-PTX30 (the number following SPION or PTX indicates the corresponding feed ratio) was obtained by lyophilization. SPION-loaded HM (HM-SPION5) and PTX-loaded HM (HM-PTX30) were prepared using an identical procedure without PTX or SPION.

### 2.3. Characterization of HM-SPION-PTX

The hydrodynamic particle size and size distribution of HM-PTX30, HM-SPION5, and HM-SPION5-PTX30 were determined using a Fiber-Optics Particle Analyzer (FPAR-1000, Otsuka electronics, Osaka, Japan). Colloidal stability was assessed in phosphate-buffered saline (PBS; pH 7.4) at 37 °C as a function of time.

The morphology of the samples was analyzed using TEM (JEM-2100F, JEOL, Tokyo, Japan). One drop of sample solution was deposited on a carbon-coated copper grid (200 mesh) and allowed to stand for 1 min. Excess solution was removed using the filter paper. The grid was dried completely and examined using TEM.

The iron contents in HM-SPION5 and HM-SPION5-PTX30 were determined using an inductively coupled plasma spectrometer (Direct Reading Echelle ICP, Teledyne Leeman Labs, NH, USA). The detector wavelength was set at 259.94 nm.

The amount of PTX in HM-PTX30 and HM-SPION5-PTX30 was determined using high-performance liquid chromatography (HPLC) [20]. For HM-SPION5-PTX30, 1 mg of the sample was dispersed in 1 ml of acetonitrile and ultracentrifuged to remove SPIONs. The supernatant of PTX in acetonitrile was collected and diluted 30-fold for analysis. HPLC analysis was performed on an Agilent 1200 series system (Agilent Technologies, Wilmington, DE, USA), using a symmetry column at 25 °C. The mobile phase was acetonitrile–water (45:55 v:v) with a flow rate of 1.0 ml/min. A diode array detector was set at 227 nm.

### 2.4. Drug release tests

The in vitro drug release profiles of PTX from HM-PTX30 and HM-SPION5-PTX30 were obtained in a PBS containing 0.8 M sodium salicylate as the medium, as reported previously [20]. HM-PTX30 or HM-SPION5-PTX30 (1 mg) was dispersed in 1 ml of PBS (pH 7.4) and placed in a cellulose ester membrane tube (MWCO = 3500). The tube was immersed in PBS containing 0.8 M sodium salicylate solution and gently shaken at 100 rpm at a 37 °C water bath. At various time intervals, the medium was refreshed. The PTX concentration was determined using a HPLC as described above.

### 2.5. In vitro MR imaging tests

In vitro $T_2$-weighted fast spin-echo images of micelles were obtained using a 1.5 T whole body clinical magnetic resonance scanner (GE Medical System, Milwaukee, WI, USA), under the following conditions: repetition time (TR) = 4500 ms, echo time (TE) = 123.6 ms, field of view (FOV) = 200 × 200 mm$^2$, flip angle = 90°. $T_2$ relaxation rates were calculated using signal intensity (SI) of regions of interest (ROI), and SI was measured using Image J software (US NIH, Bethesda, MD).

### 2.6. In vitro cytotoxicity

Squamous carcinoma SCC7 cells were from the American Type Culture Collection (Rockville, MD) and cultured in RPMI 1640 medium (Gibco, Grand Island, NY) containing 10% (v/v) fetal bovine serum and 1% (w/v) penicillin–streptomycin at 37 °C in a humidified 5% $CO_2$–95% air atmosphere. The cytotoxicity of HM-SPION5, HM-SPION5-PTX30, HM, and a Cremophor-based PTX (Cremophor EL-PTX) formulation was evaluated using the methylthiazol tetrazolium (MTT) assay. Cells were seeded at $1\times10^4$ cells/well in 96-well flat-bottomed plates. After 1 day of growth, cells were washed twice with PBS and incubated for 2 days with various concentrations of the sample. Cells were then washed twice with PBS to remove remaining drugs and fresh culture medium was added. Twenty microliters of MTT solution (5 mg/mL in PBS) was added to each well, and cells were incubated for an additional 4 h at 37 °C. Medium was removed and cells were dissolved in DMSO. The absorbance of each well was measured at 570 nm using a microplate reader (VERSAmaxTM, Molecular Devices Corp., Sunnyvale, CA).

### 2.7. In vivo MR imaging

Athymic nude mice bearing SCC7 tumors were used for in vivo MR imaging studies. Tumors were inoculated by injecting a suspension of $1\times10^6$ SCC7 cells in physiological saline (100 μl) into the subcutaneous dorsa of mice. The tumor targeting ability of HM-SPION5-PTX30 after systemic administration was investigated using a 1.5 T whole body clinical magnetic resonance scanner as described above. An aqueous dispersion of HM-SPION5-PTX30 (200 μl) was injected intravenously at a dose equivalent to 2.6 mg Fe/Kg. MR images were taken before the injection of HM-SPION5-PTX30 and at appropriate time intervals post-injection. In vivo $T_2$-weighted fast spin-echo imaging was performed under the following conditions: TR = 3500 ms, TE = 56.9 ms, FOV = $6\times6$ cm$^2$, section thickness = 0.8 mm for 12 h. SI at defined ROI was quantitatively measured using Image J software (US NIH, Bethesda, MD).

### 2.8. Antitumor efficacy of HM-SPION-PTX

To estimate the antitumor efficacy of PTX and Hy-SPION5-PTX30, subcutaneous tumors were prepared by inoculating SCC7 cells ($1\times10^6$) in the left flank of athymic nude mice (5-week-old males, $n=5$). When tumors reached approximately 80–120 mm$^3$, HM-SPION5-PTX30 micelles, PTX, or saline was intravenously injected at 20 mg PTX/kg into tumor-bearing mice once every 3 days. Tumor volumes were calculated according to the formula $V=(AB^2)\times0.52$, where $A$ is the major axis and $B$ is the minor axis.

## 3. Results and discussion

### 3.1. Preparation and physicochemical characterization of HM-SPION-PTX

An amphiphilic hydrotropic block copolymer (PEG-*b*-PVBODENA) was synthesized using PEG-Br as a macroinitiator via ATRP, as reported [20]. In previous studies, copolymers with longer DENA block lengths showed enhanced PTX solubility, suggesting that incorporating the DENA moieties at higher concentrations in the cores improves the drug solubilization capacity [19,20]. In this study, by controlling the feed molar ratio of the initiator and VBODENA, we synthesized the hydrotropic copolymer with the long DENA block (~6.5 KDa) to maximize the loading capacity of PTX.

To prepare HM-SPION-PTX, a non-covalent encapsulation procedure with a simple dialysis method was used (Fig. 1). Since the hydrotropic block of the copolymer has the hydrophobic nature, HM was expected to have the ability for encapsulation of both PTX and hydrophobic SPION.

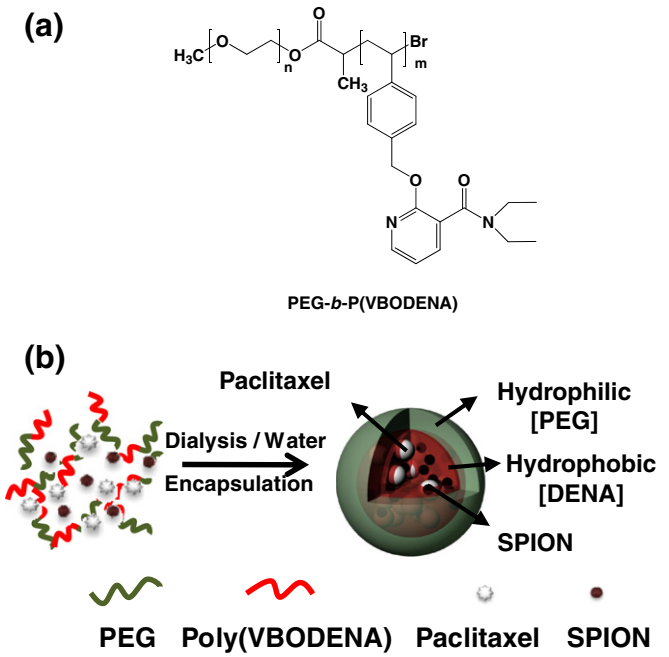


**Fig. 1.** (a) Chemical structure of PEG-*b*-PVBODENA block copolymer and (b) schematic representation for preparation of HM-SPION-PTX.

Initially, we evaluated the SPION-loading capacity of HM. When the feed ratio of SPION to HM was 0.05 to prepare HM-SPION5, the loading content and loading efficiency of SPION were 2.8% and 56.3%, respectively (Table 1). Physical encapsulation of SPION to HM increased the particular size from 68 nm to 161 nm because bulky SPIONs (6 nm in diameter) were incorporated at the inner core of HM. Although the mechanism of an increase in the particle size by encapsulation of SPION was not clearly understood, SPIONs at the core of the micelle might inhibit the effective interactions between hydrotropic blocks, resulting in formation of loose micellar core. This increase in the particle size by the small amount of SPION has been also found in other polymeric micelles [25].

An increase in the feed ratio of SPION to HM resulted in lower loading efficiency of SPION. Therefore, we fixed the feed ratio of SPION at 5%. As expected, HM was able to encapsulate a large quantity of PTX at its inner core, composed of the hydrotropic block. When the feed ratio of PTX to HM was 0.3 to obtain HM-PTX30, the loading content and loading efficiency were 21.9% and 72.88, respectively. For HM-SPION5-PTX30, the loading efficiency of SPION was comparable to HM-SPION5. However, the PTX loading capacity of HM-SPION5-PTX30 (17.5%) was slightly lower than HM-SPION30, which might be due to the presence of hydrophobic SPION in the core. Nonetheless, the drug loading content of HM-SPION5-PTX30 was significantly higher than other combined delivery systems [26,27], primarily ascribed to the hydrotropic block with hydrophobic nature.

Fig. 2 shows TEM images and particle size distributions of SPION, HM-SPION5, and HM-SPION5-PTX30. TEM results suggested that all the nanoparticles were spherical in shape with the unimodal size distribution. SPIONs, used for encapsulation into HM, were mono-disperse with a fairly uniform particle size of 6 nm. From the TEM images of HM-SPION5 and HM-SPION5-PTX30, it was found that SPIONs were uniformly embedded and formed clusters in the cores of HMs. This clustering of SPIONs in the confined environment is beneficial for MR imaging because of the increased $T_2$ relaxivity and significantly better contrast enhancement than individually dispersed nanoparticles. Other studies have verified this clustering effect in different carrier systems [8,28].

**Table 1**
Physicochemical characteristics of micelles.

| Sample | Size (nm)[a] | PTX LC (wt%)[b] | PTX LE (%) [b] | OA-SPIONs LC (wt%)[c] | OA-SPIONs LE (%)[c] | MR contrast Effect, $r_2$ ($mM^{-1}\,s^{-1}$) |
|---|---|---|---|---|---|---|
| HM | 68.2 ± 0.9 | – | – | – | – | – |
| HM-PTX30 | 85.26 ± 7.1 | 21.85 ± 0.06 | 72.83 ± 0.033 | – | – | – |
| HM-SPION5 | 161.3 ± 1.6 | – | – | 2.81 ± 0.04 | 56.27 ± 0.92 | 28.01 |
| HM-SPION5-PTX30 | 178.8 ± 1.1 | 17.50 ± 0.001 | 55.49 ± 0.005 | 2.89 ± 0.04 | 57.69 ± 0.83 | 226.76 |

[a]Particle size, measured using dynamic light scattering; [b]loading content (LC) and loading efficiency (LE) of PTX measured using HPLC; [c]LC and LE of SPION measured using ICP.

### 3.2. Relaxivity of HM-SPION-PTX

The MR imaging agent is often evaluated based on longitudinal ($r_1$) and transverse relaxivities ($r_2$) which reflect the ability of the agent to alter $T_1$ and $T_2$, respectively. Recently, increases in $r_2$ values have been shown to occur by clustering SPIONs through encapsulation of individual SPIONs within polymeric nanocarriers [4]. The resulting nanoparticle clusters exhibited better contrast enhancement and improved manipulation under external magnetic fields [28]. Fig. 3 shows the $T_2$ relaxation rates as a function of the iron concentration. The results for HM-SPION5 and HM-SPION5-PTX30 indicated linear relationships between the transverse relaxation rate and Fe concentrations. It is noteworthy that HM-SPION5-PTX30 revealed considerably enhanced contrast efficiency, as demonstrated by the much larger slope of the plot compared to that for HM-SPION5. The $r_2$ values for HM-SPION5 and HM-SPION5-PTX30 were 28.0 and 226.8 $mM^{-1}\,s^{-1}$, respectively. This suggests that the $r_2$ value of nanoparticles is significantly affected by incorporation of PTX in the core of HM, ascribed to the change in the nature of the local environment [29]. Overall, HM-SPION5-PTX30 micelles might have a potential as efficient $T_2$ contrast agents for MR imaging.

### 3.3. Stability and drug release behavior

Besides improving loading contents, another advantage of hydrotropic DENA-based drug carriers is enhanced stability after high drug loading [20,22,23]. This enhanced stability might result from high compatibility between the core-forming blocks and the drugs. In other words, increased interactions between the DENA blocks and PTX might improve the hydrophobicity of the cores and the stability of the resulting micelles. In this study, the stabilities of HM, HM-PTX30, HM-SPION5, and HM-SPION5-PTX30 at physiological conditions (PBS 7.4, 37 °C) were evaluated by monitoring changes in the particular size as a function of time. As shown in Fig. 4a, all the nanoparticles were fairly stable for at least 6 days, and no precipitate was observed (see Supplementary Information, Fig. S1).

In vitro drug release behaviors of HM-PTX30 and Hy-SPION5-PTX30 were evaluated in 0.8 M sodium salicylate as a dissolution medium. Sodium salicylate has been demonstrated to be a suitable agent for PTX release experiments, compared to organic solvents and surfactants which can affect the physical integrity of the carrier structure [19]. In general, the release characteristics of drugs from micelles are influenced by parameters such as amount of loaded drug, block lengths, and interactions between drugs and core-forming blocks [30]. In this study, release behavior of PTX from HM-SPION5-PTX30 was evaluated and compared with that from HM-PTX30 to determine if SPIONs affected the release of PTX from HM. As shown in Fig. 4b, both micelles released PTX in a sustained manner and the release pattern of Hy-SPION5-PTX30 was comparable to that of HM-PTX30 [19,31]. More than 80% of PTX was released from HMs within 10 h. Overall, these results suggested that HM-SPION5-PTX30 has the potential to release the PTX in a sustained manner, and the presence of SPIONs in the micelle cores did not significantly affect the release characteristics of the resulting micelles.

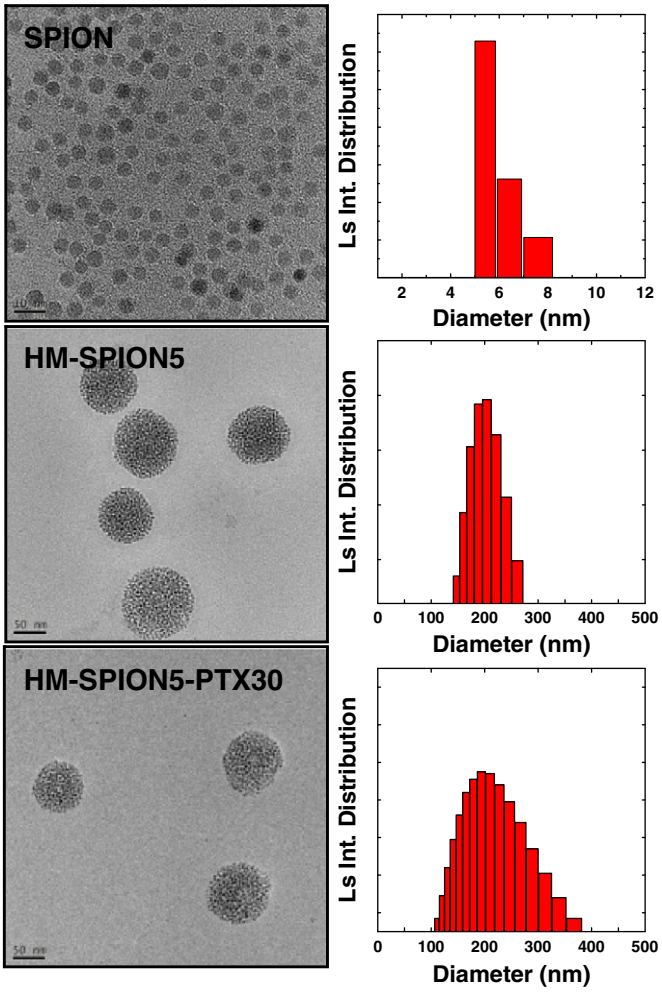


**Fig. 2.** TEM image and particle size distribution of SPION and micelles.

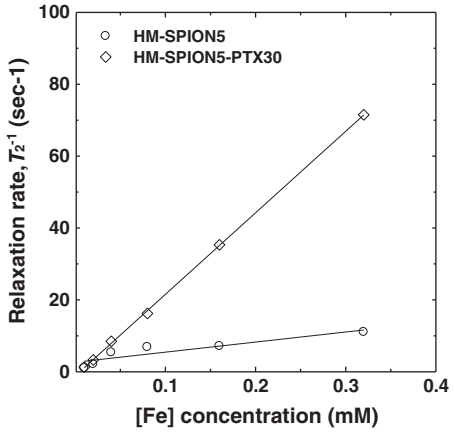


**Fig. 3.** $T_2$ relaxation rates as a function of iron concentration.

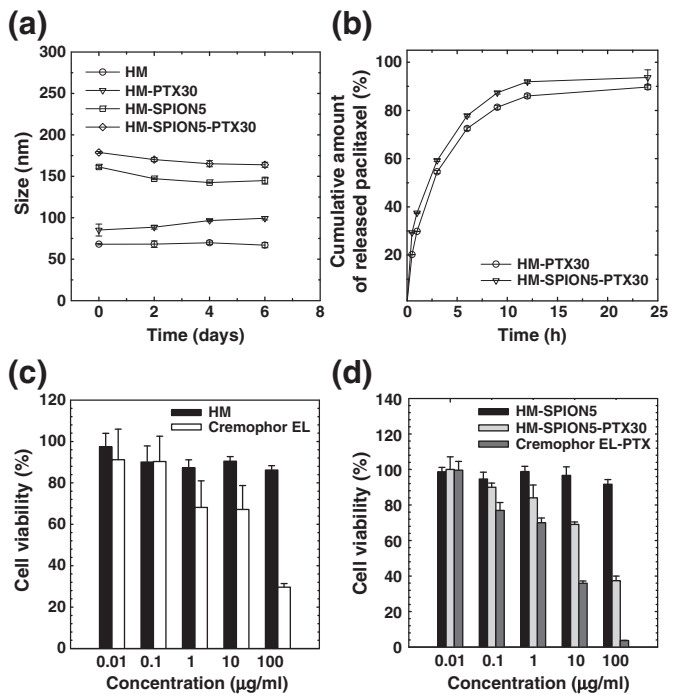


**Fig. 4.** (a) Particle size of micelles at PBS (pH 7.4; 37 °C) as a function of time, (b) release profile of PTX from micelles, and in vitro cytotoxicity of (c) vehicles and (d) active agent-loaded samples. Error bars represent standard deviations ($n = 5$).

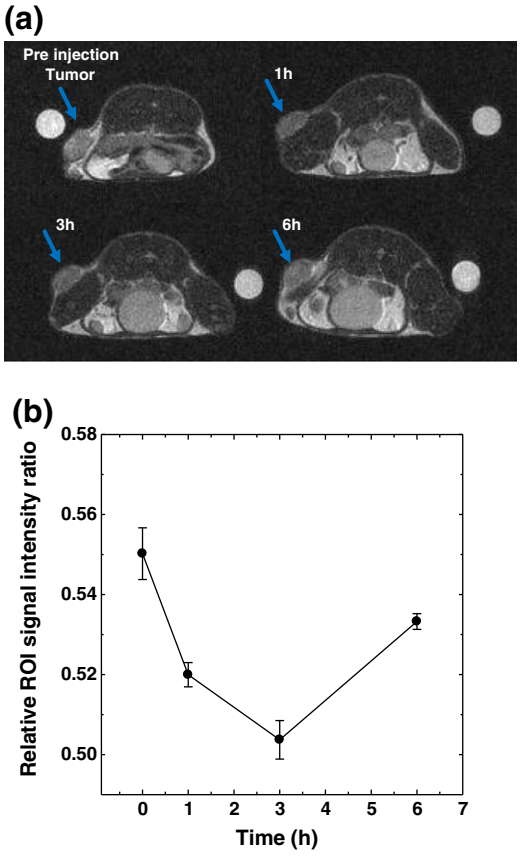


**Fig. 5.** (a) In vivo $T_2$-weighted MR images before and after injection of 2.6 mg Fe $Kg^{-1}$ of HM-SPION5-PTX30 to a tumor-bearing mouse. Arrow indicates the tumor region. (b) Change of signal intensity ratios between the region of the interest and PBS at different time intervals after systemic administration of HM-SPION5-PTX30. Error bars represent standard deviations ($n = 3$).

### 3.4. In vitro cytotoxicity

The cytotoxic effects of HM, HM-SPION5 and HM-SPION5-PTX30 on SCC7 cells were evaluated using an MTT colorimetric assay. The cytotoxicities of free PTX in a 50:50 v/v mixture of Cremophor EL/ethanol (a clinical vehicle for taxol) and vehicle alone were also assessed as controls. As shown in Fig. 4c, HM maintained cell viability even at higher concentrations, whereas the Cremophor EL vehicle showed considerable toxicity at high concentrations. These results suggest that HM as a carrier is nontoxic to SCC7 cells. This is in agreement with previous studies, which demonstrated no significant toxicities to other human cancer cell lines such as HT-29, MDA231, MCF-7 and SKOV-3 [20]. Most of cells were viable at all the concentrations of HM-SPION5, indicating no significant toxicity of SPIONs in HM (Fig. 4d). Unlike other inorganic nanoparticles, SPIONs have shown an excellent biocompatibility and biodegrade into nonmagnetic iron metabolites in the body [32]. Therefore, HMs loaded with only SPIONs were not expected to affect cell viability at the tested concentrations. On the other hand, HM-SPION5-PTX30 showed dose-dependent cytotoxicity, ascribed to release of PTX from micelles. It is noteworthy that PTX showed higher cytotoxicity than HM-SPION5-PTX30 at the same concentrations of PTX, which might be due to the sustained release of PTX from HM-SPION5-PTX30.

### 3.5. In vivo MR imaging of HM-PTX5-SPION30

HM-SPION5-PTX30, prepared in this study, is not functionalized with tumor-homing moieties. However, the presence of the PEG shell may permit the micelles to circulate in the bloodstream long enough to accumulate at the tumor, by exploiting the leaky vasculature and poor lymphatic drainage around tumors via an EPR effect [33]. To test the tumor targetability of our micelles, HM-SPION5-PTX30 micelles were systemically administered to tumor-bearing mice and their time-dependent accumulation at the tumor site monitored using MR imaging. As shown in Fig. 5a, a noticeable darkening in $T_2$-weighted images was observed at the tumor site at 1 hour post-injection, implying accumulation of micelles at the tumors. We also quantitatively determined SI ratios between ROI and PBS at different intervals after systemic administration of HM-SPION5-PTX30. The result showed the decrease in a tumor-selective SI 1 hour after injection, with a maximal signal drop at 3 h post-injection (Fig. 5b). Afterwards, signals regained slowly, suggesting that the micelles were gradually cleared from the tumors. In general, the accumulation and clearance rate of micelles or any nanoparticles at tumors depend on factors such as the particular size and surface characteristics of the nanoparticles, their half-lives in vivo, and permeability of the tumor vasculature. Other studies demonstrated that pluronic and PEG-based amphiphilic copolymer-coated SPIONs exhibit maximum tumor accumulation at 3 h after injection, with subsequent excretion through visceral organs such as the kidneys [34]. Thus, our in vivo results indicated that HM-SPION5-PTX30 micelles effectively reached the tumor site and produced sufficient contrast effects for MR imaging.

### 3.6. In vivo anticancer efficacy of HM-PTX5-SPION30

The in vivo therapeutic effect of HM-SPION5-PTX30 on tumor was evaluated using SCC7 tumor-bearing mice. Mice were injected with HM-SPION5-PTX30 (20 mg PTX/kg), Cremophor EL-PTX (20 mg PTX/kg), or saline. As shown in Fig. 6a, no significant differences in tumor sizes were observed among the three groups for up to 4 days. After 8 days, tumor growth was effectively inhibited in animals treated with HM-SPION5-PTX30, indicating that the integrated micellar formulation was more effective in inhibiting tumor growth than the Cremophor EL-PTX formulation. Histological studies supported the antitumor effects. As shown in Fig. 6b, mice treated with HM-SPION5-PTX30

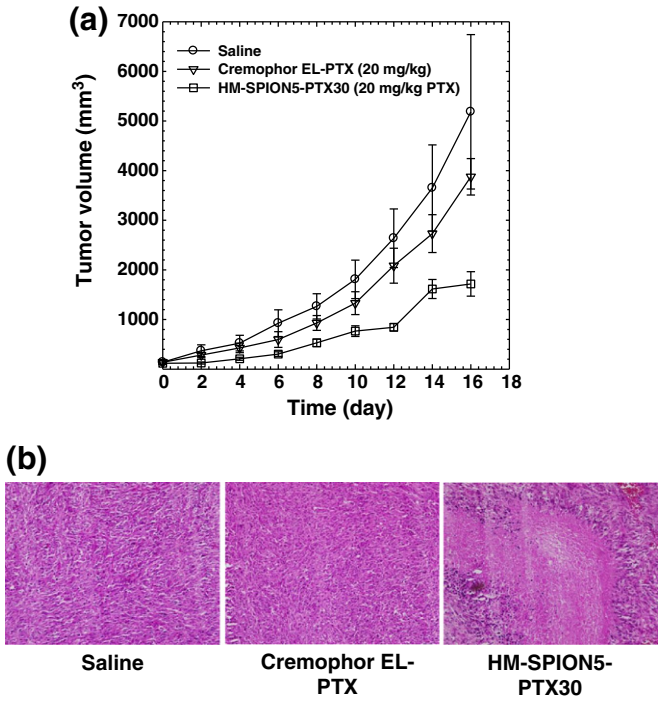


**Fig. 6.** (a) Antitumor efficacy of HM-SPION5-PTX30 and Cremophor EL-PTX in SCC7 tumor-bearing mice. (b) Histological images of the tumor tissues using H&E staining. Error bars represent standard deviations ($n = 5$).

showed decreases in tumor cells compared to saline and Cremophor EL-PTX groups. Overall, these results suggest that HM-SPION5-PTX30 possesses high antitumor activity and have the potential as the contrast agent for MR imaging of tumor. Therefore, HM-SPION5-PTX30 might be useful as theranostic nanoparticles for cancer treatment.

## 4. Conclusion

This study examined the potential of hydrotropic polymer micelles as a single-platformed carrier for combined delivery of imaging agents and drugs. HM could encapsulate both PTX and SPION with high loading efficacies. Considering the enhanced loading capabilities and the ability to accumulate at tumors, this single-platformed hydrotropic polymer micelle might be useful for simultaneous diagnosis and treatment of cancer.

Supplementary data to this article can be found online at http://dx.doi.org/10.1016/j.jconrel.2012.04.012.

## Acknowledgements

This work was financially supported by the Korea Healthcare Technology R&D Project (A101706-1001-0000200) of MW, the Global Research Laboratory (GRL) Project, the Converging Research Program (20090081876), and the Basic Science Research Program (20100027955) of MEST.

## References

[1] J. Xie, S. Lee, X. Chen, Nanoparticle-based theranostic agents, Adv. Drug Deliv. Rev. 62 (2010) 1064–1079.
[2] K. Park, S. Lee, E. Kang, K. Kim, K. Choi, I.C. Kwon, New generation of multifunctional nanoparticles for cancer imaging and therapy, Adv. Funct. Mater. 19 (2009) 1553–1566.
[3] K. Kim, J.H. Kim, H. Park, Y.-S. Kim, K. Park, H. Nam, S. Lee, J.H. Park, R.-W. Park, I.-S. Kim, K. Choi, S.Y. Kim, K. Park, I.C. Kwon, Tumor-homing multifunctional nanoparticles for cancer theragnosis: simultaneous diagnosis, drug delivery, and therapeutic monitoring, J. Control. Release 146 (2010) 219–227.
[4] N. Nasongkla, E. Bey, J. Ren, H. Ai, C. Khemtong, J.S. Guthi, S.-F. Chin, A.D. Sherry, D.A. Boothman, J. Gao, Multifunctional polymeric micelles as cancer-targeted, mri-ultrasensitive drug delivery systems, Nano Lett. 6 (2006) 2427–2430.
[5] T.P. Thomas, I.J. Majoros, A. Kotlyar, J.F. Kukowska-Latallo, A. Bielinska, A. Myc, J.R. Baker, Targeting and inhibition of cell growth by an engineered dendritic nanodevice, J. Med. Chem. 48 (2005) 3729–3735.
[6] M. de Smet, S. Langereis, S.v. den Bosch, H. Grüll, Temperature-sensitive liposomes for doxorubicin delivery under mri guidance, J. Control. Release 143 (2010) 120–127.
[7] C. Sanson, O. Diou, J. Thévenot, E. Ibarboure, A. Soum, A. Brûlet, S. Miraux, E. Thiaudière, S. Tan, A. Brisson, V. Dupuis, O. Sandre, S. Lecommandoux, Doxorubicin loaded magnetic polymersomes: theranostic nanocarriers for MR imaging and magneto-chemotherapy, ACS Nano 5 (2011) 1122–1140.
[8] J. Kim, J.E. Lee, S.H. Lee, J.H. Yu, J.H. Lee, T.G. Park, T. Hyeon, Designed fabrication of a multifunctional polymer nanomedical platform for simultaneous cancer- targeted imaging and magnetically guided drug delivery, Adv. Mater. 20 (2008) 478–483.
[9] C. Oerlemans, W. Bult, M. Bos, G. Storm, J. Nijsen, W. Hennink, Polymeric micelles in anticancer therapy: targeting, imaging and triggered release, Pharm. Res. 27 (2010) 2569–2589.
[10] S. Kaida, H. Cabral, M. Kumagai, A. Kishimura, Y. Terada, M. Sekino, I. Aoki, N. Nishiyama, T. Tani, K. Kataoka, Visible drug delivery by supramolecular nanocarriers directing to single-platformed diagnosis and therapy of pancreatic tumor model, Cancer Res. 70 (2010) 7031–7041.
[11] J.L. Turner, D.P.J. Pan, R. Plummer, Z.Y. Chen, A.K. Whittaker, K.L. Wooley, Synthesis of gadolinium-labeled shell-crosslinked nanoparticles for magnetic resonance imaging applications, Adv. Funct. Mater. 15 (2005) 1248–1254.
[12] G. Zhang, R. Zhang, X. Wen, L. Li, C. Li, Micelles based on biodegradable poly(l-glutamic acid)-b-polylactide with paramagnetic gd ions chelated to the shell layer as a potential nanoscale mri−visible delivery system, Biomacromolecules 9 (2007) 36–42.
[13] O. Veiseh, J.W. Gunn, M. Zhang, Design and fabrication of magnetic nanoparticles for targeted drug delivery and imaging, Adv. Drug Deliv. Rev. 62 (2010) 284–304.
[14] H. Ai, C. Flask, B. Weinberg, X.T. Shuai, M.D. Pagel, D. Farrell, J. Duerk, J. Gao, Magnetite-loaded polymeric micelles as ultrasensitive magnetic-resonance probes, Adv. Mater. 17 (2005) 1949–1952.
[15] S. Kim, Y. Shi, J.Y. Kim, K. Park, J.-X. Cheng, Overcoming the barriers in micellar drug delivery: loading efficiency, in vivo stability, and micelle–cell interaction, Expert Opin. Drug Deliv. 7 (2010) 49–62.
[16] X. Yang, J.J. Grailer, I.J. Rowland, A. Javadi, S.A. Hurley, V.Z. Matson, D.A. Steeber, S. Gong, Multifunctional stable and ph-responsive polymer vesicles formed by heterofunctional triblock copolymer for targeted anticancer drug delivery and ultrasensitive mr imaging, ACS Nano 4 (2010) 6805–6817.
[17] G.H. Gao, J.W. Lee, M.K. Nguyen, G.H. Im, J. Yang, H. Heo, P. Jeon, T.G. Park, J.H. Lee, D.S. Lee, pH-responsive polymeric micelle based on PEG-poly(β-amino ester)/(amido amine) as intelligent vehicle for magnetic resonance imaging in detection of cerebral ischemic area, J. Control. Release 155 (2011) 11–17.
[18] D. Chen, N. Li, X. Xia, Q. Xu, J. Ge, Y. Li, J. Lu, H. Gu, pH-responsive polymeric-cargo encapsulated magnetic nanoparticles for selective release and imaging, J. Control. Release 152 (Supplement 1) (2011) e67–e68.
[19] K.M. Huh, S.C. Lee, Y.W. Cho, J. Lee, J.H. Jeong, K. Park, Hydrotropic polymer micelle system for delivery of paclitaxel, J. Control. Release 101 (2005) 59–68.
[20] S.C. Lee, K.M. Huh, J. Lee, Y.W. Cho, R.E. Galinsky, K. Park, Hydrotropic polymeric micelles for enhanced paclitaxel solubility: in vitro and in vivo characterization, Biomacromolecules 8 (2007) 202–208.
[21] J. Lee, S.C. Lee, G. Acharya, C.J. Chang, K. Park, Hydrotropic solubilization of paclitaxel: analysis of chemical structures for hydrotropic property, Pharm. Res. 20 (2003) 1022–1030.
[22] G. Saravanakumar, K.H. Min, D.S. Min, A.Y. Kim, C.M. Lee, Y.W. Cho, S.C. Lee, K. Kim, S.Y. Jeong, K. Park, J.H. Park, I.C. Kwon, Hydrotropic oligomer-conjugated glycol chitosan as a carrier of paclitaxel: synthesis, characterization, and in vivo biodistribution, J. Control. Release 140 (2009) 210–217.
[23] G. Saravanakumar, K.Y. Choi, H.Y. Yoon, K. Kim, J.H. Park, I.C. Kwon, K. Park, Hydrotropic hyaluronic acid conjugates: synthesis, characterization, and implications as a carrier of paclitaxel, Int. J. Pharm. 394 (2010) 154–161.
[24] J. Park, K. An, Y. Hwang, J.-G. Park, H.-J. Noh, J.-Y. Kim, J.-H. Park, N.-M. Hwang, T. Hyeon, Ultra-large-scale syntheses of monodisperse nanocrystals, Nat. Mater. 3 (2004) 891–895.
[25] M. Talelli, C.J.F. Rijcken, T. Lammers, P.R. Seevinck, G. Storm, C.F. van Nostrum, W.E. Hennink, Superparamagnetic iron oxide nanoparticles encapsulated in biodegradable thermosensitive polymeric micelles: toward a targeted nanomedicine suitable for image-guided drug delivery, Langmuir 25 (2009) 2060–2067.
[26] T.K. Jain, J. Richey, M. Strand, D.L. Leslie-Pelecky, C.A. Flask, V. Labhasetwar, Magnetic nanoparticles with dual functional properties: drug delivery and magnetic resonance imaging, Biomaterials 29 (2008) 4012–4021.
[27] X. Yang, Y. Chen, R. Yuan, G. Chen, E. Blanco, J. Gao, X. Shuai, Folate-encoded and fe3o4-loaded polymeric micelles for dual targeting of cancer cells, Polymer 49 (2008) 3477–3485.
[28] P. Qiu, C. Jensen, N. Charity, R. Towner, C. Mao, Oil phase evaporation-induced self-assembly of hydrophobic nanoparticles into spherical clusters with controlled surface chemistry in an oil-in-water dispersion and comparison of behaviors of individual and clustered iron oxide nanoparticles, J. Am. Chem. Soc. 132 (2010) 17724–17732.
[29] D. Cheng, G. Hong, W. Wang, R. Yuan, H. Ai, J. Shen, B. Liang, J. Gao, X. Shuai, Nonclustered magnetite nanoparticle encapsulated biodegradable polymeric micelles with enhanced properties for in vivo tumor imaging, J. Mater. Chem. 21 (2011) 4796–4804.
[30] A. Lavasanifar, J. Samuel, G.S. Kwon, Poly(ethylene oxide)-block-poly(−amino acid) micelles for drug delivery, Adv. Drug Deliv. Rev. 54 (2002) 169–190.

[31] H. Kang Moo, M. Hyun Su, L. Sang Cheon, L. Hong Jae, K. Sungwon, P. Kinam, A new hydrotropic block copolymer micelle system for aqueous solubilization of paclitaxel, J. Control. Release 126 (2008) 122–129.
[32] T.K. Jain, M.K. Reddy, M.A. Morales, D.L. Leslie-Pelecky, V. Labhasetwar, Biodistribution, clearance, and biocompatibility of iron oxide magnetic nanoparticles in rats, Mol. Pharm. 5 (2008) 316–327.
[33] L. van Vlerken, T. Vyas, M. Amiji, Poly(ethylene glycol)-modified nanocarriers for tumor-targeted and intracellular delivery, Pharm. Res. 24 (2007) 1405–1414.
[34] J. Park, M.K. Yu, Y.Y. Jeong, J.W. Kim, K. Lee, V.N. Phan, S. Jon, Antibiofouling amphiphilic polymer-coated superparamagnetic iron oxide nanoparticles: synthesis, characterization, and use in cancer imaging in vivo, J. Mater. Chem. 19 (2009) 6412–6417.